Journal of Solid State Chemistry 184 (2011) 1245–1250

Contents lists available at ScienceDirect

Journal of Solid State Chemistry

journal homepage: www.elsevier.com/locate/jssc

Selective decoration of nickel and nickel oxide nanocrystals on multiwalled carbon nanotubes

P. Martis, B.R. Venugopal, J. Delhalle, Z. Mekhalif*

Laboratoire de Chimie et d'Electrochimie des Surface, Facultés Universitaires Notre-Dame de la Paix, 61 Rue de Bruxelles, B-5000, Namur, Belgium

ARTICLE INFO

Article history:
Received 12 January 2011
Received in revised form
16 March 2011
Accepted 18 March 2011
Available online 23 March 2011

Keywords:
Nickel
Nickel oxide
Nanocrystal
Multiwalled carbon nanotube
Calcination

ABSTRACT

A simple route to selective decoration of nickel and nickel oxide nanocrystals on multiwalled carbon nanotubes (MWCNTs) using nickel acetylacetonate (NAA) was successfully achieved for the first time. The homogeneously decorated nanocrystals on MWCNTs were investigated for their structure and morphology by various techniques, such as powder X-ray diffraction, Fourier transform infrared spectroscopy, X-ray photoelectron spectroscopy, transmission electron microscopy, field emission scanning electron microscopy and thermogravimetric analysis. It was found that the size distributions of the nanocrystals on MWCNTs ranged from 8 to 15 nm and they were well resolved. The precursor, NAA, was effectively employed to impregnate the MWCNTs, which on calcination at suitable temperatures and in the presence of hydrogen and nitrogen atmosphere gave rise to nickel and nickel oxide nanocrystals, respectively.

1. Introduction

The external surface modification of CNTs and anchoring of metal or metal oxide nanoparticles on them can dramatically influence their physical, mechanical, thermal and electrical properties, which may lead to novel changes that are relevant to potential applications in diverse fields, such as catalysis, chemical/biological sensing and optoelectronics [1–10]. It has been found that the binding energy between metals and pristine CNTs is rather small [11], resulting in poor metal–CNT adhesion. If the adhesion between the metal and the CNTs is not strong, the benefits of the high tensile strength of CNTs are lost. One principle way to increase the surface reactivity of CNTs is by the inclusion of defects and functional groups on CNTs. The binding energies between CNT and transition metals are found to be significantly enhanced when vacancy defects are introduced into the CNTs [12].

Since CNTs are known to be largely inert, it is necessary to create defect and active sites to anchor metal particles on the external surface of CNTs. Oxidation of CNTs by strong acids is a well-known strategy to create functional groups like carboxylic (–COOH), carbonyl (–CO) and hydroxylic (–OH) [13–19]. This changes the reactivity of nanotubes and modifies the wetting characteristics, which would enrich their properties. It leads us to the issue of interfacial bonding between the metal atoms and defective and oxidized CNTs to ensure excellent mechanical performances for the CNT-reinforced metal-matrix composites. It is suggested that these stable CNT–metal systems could become promising engineering materials in many fields such as CNT devices for various spintronics applications and CNT metal-matrix composites [20–22]. So far, Ni/CNT nano-composites have been considered for use in many energy related applications such as fuel cells, rechargeable batteries, super capacitors and hydrogen production [23–25].

Many researchers have attempted to produce metal/metal oxide and CNT composites; however, the difficulty of obtaining a uniform coating on CNTs imposes limitations. Sometimes prior to the decoration of metal/metal oxides, the CNTs are modified with polymer to facilitate the process [2,3]. For example, Tang et al. [2] reports the distribution of Ni nanoparticles on poly (acrylic acid) modified MWCNTs for hydrogenation of α, β-unsaturated aldehyde. Similarly homogeneous electrodeposition of Ni nanoparticles on 4-nitroaniline radical monolayer grafted on MWCNT was reported by Jin et al. [3]. There have been reports of employing stringent conditions such as microwave irradiation [26], hydrothermal [27], solvothermal [28], chemical vapor deposition [29], electrophoretic deposition [30], etc. for the uniform distribution of metal/metal oxides on CNTs.

Keeping in mind the potential applications of the CNT based composites with metal/metal oxides such as Ni/NiO and the complexity involved in achieving their uniform distribution we report a simple and convenient method for the preparation of nickel and nickel oxide nanoparticles well dispersed on MWCNTs. Our purpose is to establish a novel and a low cost alternative route for coating the external surface of MWCNTs with metal and metal oxide nanoparticles of nickel. In this context, nickel acetylacetonate (NAA) was used, for the first time, as the

* Corresponding author. Fax: +32 81 72 46 00.
E-mail address: zineb.mekhalif@fundp.ac.be (Z. Mekhalif).

0022-4596/$ - see front matter © 2011 Elsevier Inc. All rights reserved.
doi:10.1016/j.jssc.2011.03.036

precursor to decorate on MWCNTs. The weight percentage ratio of NAA to CNTs, impregnation time, reaction temperature and atmosphere are selectively controlled to obtain the amount, particle size and homogeneous distribution of nickel/nickel oxide particles on CNTs. Moreover, the MWCNTs with metal coatings have significant potential for a fabrication of new powdery metal–MWCNT composites, thus extending their applications.

2. Material and methods

All the chemicals used were of analytical grade and used without further purification. Nickel acetylacetonate of 96% purity was procured from Acros Organics, USA. The thin MWCNTs, obtained from Nanocyl S.A. Belgium, were synthesized by decomposition of ethylene using the CCVD method. The MWCNTs have an average diameter of 10 nm and length of several (0.1–10) micrometers. The purity of the MWCNTs was more than 95%.

2.1. Oxidation of thin MWCNTs

The oxygen functionalities were generated on surface of thin MWCNTs by treating them with the mixture of concentrated H_2SO_4 and HNO_3 with a molar ratio of 3:1 following the method reported in the literature [17,18]. In a typical experiment 75 ml of conc. H_2SO_4 (97%) and 25 ml of conc. HNO_3 (65%) were carefully mixed together and added to 1 g of MWCNTs in a round bottomed flask. The above suspension was then heated under constant agitation at 50 °C for 8 h. Afterwards the mixture was allowed to cool down to room temperature, added to equal quantity of deionized water, filtered and the residue was washed several times with deionised water until neutral pH was attained. The residue was then filtered and freeze-dried. The oxidized MWCNTs will be hereafter referred to as O-MWCNTs.

2.2. Impregnation of NAA on O-MWCNTs

100 mg of O-MWCNTs was sonicated in 50 ml of xylene until (~5 min) a good suspension is obtained. Similarly suspension of NAA in xylene was obtained by sonicating 77.2 mg of NAA (15 wt% of Ni) in 30 ml of xylene for the same amount of time. While the suspensions were still under ultrasonication, NAA in xylene was added to the O-MWCNTs in xylene suspension. The mixture was further sonicated for a few minutes. The mixture was then refluxed under magnetic stirring for 4 h and cooled to room temperature, filtered and the residue was washed three times with acetone. The NAA impregnated MWCNTs thus obtained, designated as NAA-MWCNTs hereafter, were finally dried at room temperature in air.

2.3. Calcination of NAA-MWCNTs

The NAA-MWCNTs was then calcined in a tubular furnace equipped with quartz tube pre- heated to a desired temperature under the continuous flow of either nitrogen/hydrogen at a flow rate of 300 μL per min. In a typical experiment, 20 mg of NAA-MWCNTs was calcined at 400 °C for 1 h under continuous flow of hydrogen or for 3 h under continuous flow of nitrogen.

2.4. Characterization

Various techniques were used to characterize the impregnated and calcined materials. The phase purity of the materials were determined by powder X-ray powder diffraction (PXRD) analysis using PHILIPS-7602EA diffractometer operating with 40 kV of voltage and 30 mA of tube current with Cu $K\alpha$ radiation (λ=1.5418 Å) in the 2θ range of 10–80°. Fourier transform infrared (FTIR) spectra were recorded on a Perkin Elmer Spectrum 65 FT-IR Spectrometer. The trace amount of the sample was added to prepare the KBr pellets, which was then employed for the characterization. X-ray photoelectron spectroscopy (XPS) spectra were recorded at 35° take-off angle (relative to the surface normal) with an SSX-100 spectrometer using monochromatized Al $K\alpha$ radiation (1486.6 eV). The analyzed core-level lines were calibrated with respect to the component C 1 s of binding energy set at 284.6 eV. The surface morphology of the materials were studied by field-emission scanning electron microscopy (FE-SEM) using JEOL JSM-7500 F microscope operating at 20 kV at a working distance of 8 mm equipped with energy dispersive X-ray (EDX) analysis facility. The particle size and distribution of Ni/NiO particles on MWCNTs were studied by low resolution TEM using a TECNAI 10 PHILIPS microscope. Prior to the analysis, the samples were dispersed in ethanol and a drop of the suspension was deposited on a holey carbon-coated copper grid. Thermogravimetric analysis (TGA) measurements were performed on a METTLER TOLEDO TGA/SDTA 851e. The samples were heated from 30 to 800 °C at a heating rate of 10 °C/min in nitrogen. The residual mass loss was recorded as a function of temperature.

3. Results and discussion

The thin MWCNTs were oxidized to create active sites to anchor nanoparticles on their walls and were investigated by FTIR as shown in Fig. 1. The peak, for pristine MWCNTs (Fig. 1a), observed around 3433 cm^{-1} is attributed to O–H stretching frequency, originating from the adsorbed water molecules on the amorphous carbon in the CNTs [31]. The two peaks at 1622 and 1381 cm^{-1} are assigned to C=C stretching frequency is due to the inherent structure of CNTs. In case of O-MWCNTs (Fig. 1b), there is an

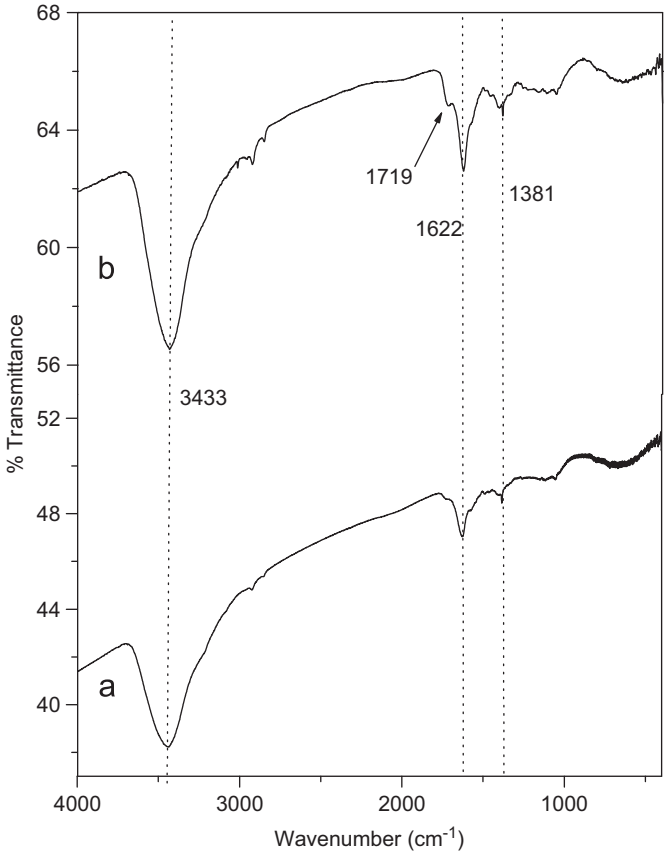

Fig. 1. FTIR spectra of (a) pristine MWCNTs and (b) O-MWCNTs.

additional peak observed at 1719 cm^{-1} which is due to the C=C stretching frequency, indicating the presence of carboxylic groups created during the oxidation of pristine MWCNTs. Further, the increased intensity in the peak observed around 3433 cm^{-1} is attributed to O–H stretching frequency, obtained due to the adsorbed water molecules and the oxidation of MWCNTs, following the acid treatment performed on pristine MWCNTs.

The PXRD patterns of the O-MWCNTs, NAA-MWCNTs along with the calcined products of NAA-MWCNTs in hydrogen and nitrogen atmosphere are shown in Fig. 2. The O-MWCNTs (Fig. 2a) display two distinct diffraction peaks for graphitic structure at $2\theta=26^\circ$ and 43° corresponding to the *hkl* reflections (0 0 2) and (1 0 0), respectively. They are the characteristic peaks for the CNTs, which indicate that even after the vigorous treatment of CNTs in concentrated acids the graphitic structure remained mainly intact. PXRD pattern of the NAA impregnated MWCNTs (Fig. 2b) is similar to that of the O-MWCNTs. This may be due to the amorphous nature of the impregnated NAA before calcinations [32]. Fig. 2c reveals the formation of the phase pure NiO nanocrystals, having three distinct diffraction peaks at $2\theta=36.9^\circ$, 42.8° and 62.3° corresponding to the *hkl* reflections (1 1 1), (2 0 0) and (2 2 0), on the surface of MWCNTs in the NiO-MWCNT composites [3]. It was obtained in the presence of nitrogen atmosphere at 400 °C. In the presence of hydrogen atmosphere at 400 °C, the two distinct diffraction peaks were obtained at $2\theta=44.2^\circ$ and 51.7° (Fig. 2d) corresponding to the *hkl* reflections (1 1 1) and (2 0 0), respectively, indicate the formation of phase pure Ni nanocrystals in the Ni-MWCNT composites [3]. Both the composites show MWCNT peaks in spite of them being treated at high temperatures in the presence of metal/metal oxide nanocrystals, which show that CNT structure is kept intact. In all the cases, no peaks other than nickel and nickel oxide are seen,

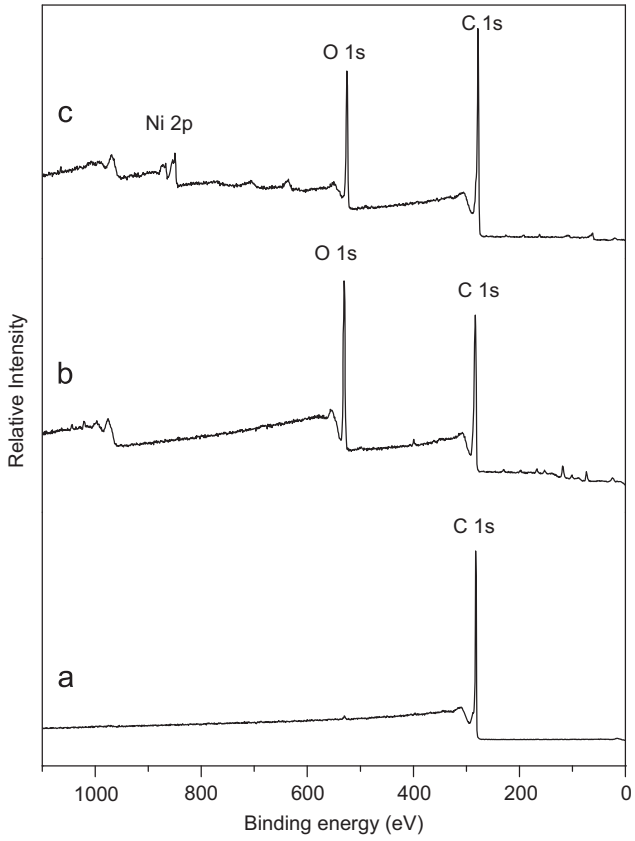

Fig. 3. XPS spectra of (a) pristine MWCNTs, (b) O-MWCNTs and (c) NAA-MWCNTs.

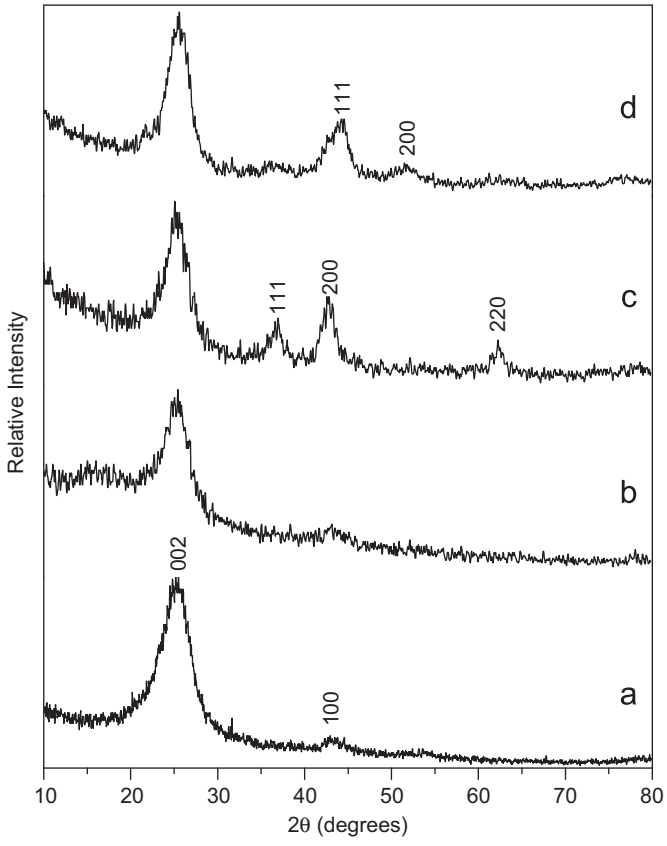

Fig. 2. PXRD patterns of (a) O-MWCNTs, (b) NAA-MWCNTs, (c) NiO-MWCNTs and (d) Ni-MWCNTs.

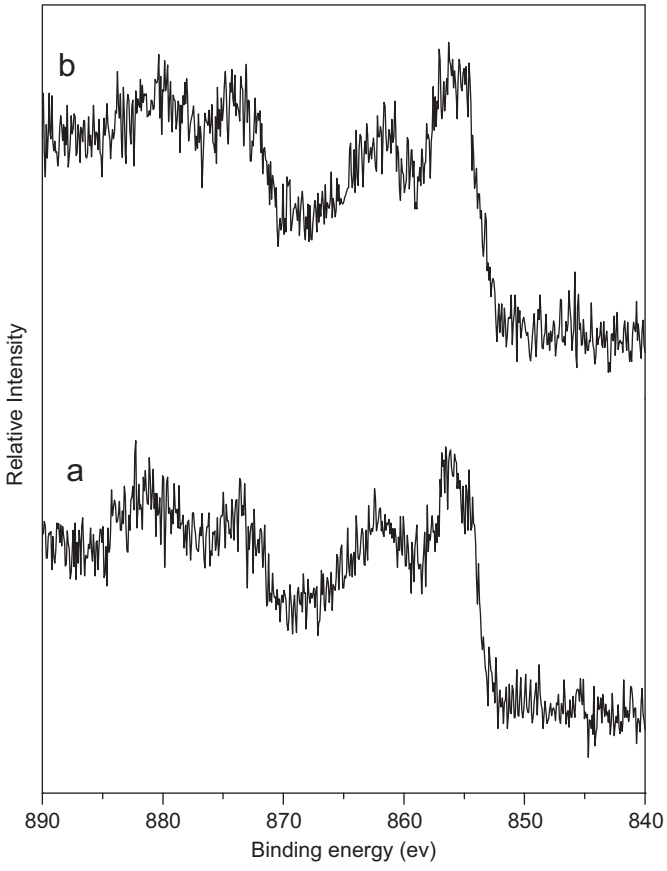

Fig. 4. High resolution XPS spectra of core Ni 2*p* of the calcined products (a) NiO-MWCNTs and (b) Ni-MWCNTs.

indicating that there are no impurities formed during the composite formation.

To further understand the extent of oxidation of MWCNTs and the composition of the final products, XPS was performed. Fig. 3 shows the XPS general survey spectra of purified MWCNTs, O-MWCNTs and NAA-MWCNTs. The oxidation of CNTs and the impregnation of NAA on the walls of the oxygenated CNTs are confirmed by the presence of the O 1*s* (Fig. 3b) and Ni 2*p* peaks (Fig. 3c). It was calculated from the XPS spectrum, for O-MWCNTs (Fig. 3b), and found that there was about 26% of oxygen in comparison to 74% carbon on the surface of O-MWCNTs. These results corroborate the FTIR investigations done on O-MWCNTs, previously (Fig. 1b). The high resolution XPS spectra for Ni 2*p* core level for the calcined products recorded in the range of 840–890 eV are shown in Fig. 4. For NiO-MWCNTs (Fig. 4a), the presence of most intense peak at 856 eV, corresponding to the binding energy of Ni $2p_{3/2}$ along with an intense satellite peaks at the higher binding energy side of the main peaks is due to the presence of NiO in the composite which agrees well with the literature report [33,34]. The presence of NiO related peaks in Fig. 4b is due to the presence of thin NiO layer on the surface of Ni in the composites, which is usually observed due to surface passivation [35]. Since the formation of NiO layer is very thin, it is not detected in the XRD pattern of Ni-MWCNTs (Fig. 2d) composite.

The morphology of the composites was investigated by FEG-SEM and TEM analysis as shown in Fig. 5. Fig. 5a, b and c are the FEG-SEM images of NAA-MWCNTs, Ni-MWCNTs and NiO-MWCNTs, respectively, which reveal the undamaged structure of MWCNTs in the composites. In both FEG-SEM and TEM images of NAA-MWCNTs (Fig. 5a and a1) the impregnated NAA species are not well-formed. The distinct and uniformly spread nickel nanocrystals on the external surface of MWCNTs in Fig. 5b demonstrates that the new approach of calcining the NAA-MWCNTs at 400 °C in the presence of hydrogen to form Ni-MWCNTs is effective.

In case of NiO-MWCNTs (Fig. 5c), although the size of the particles is similar, the particle distribution is more dense compare to Ni-MWCNTs (Fig. 5b). TEM images of NAA-MWCNTs, Ni-MWCNTs and NiO-MWCNTs are shown in Fig. 5a1, b1 and c1, respectively. The particle sizes of nickel in Ni-MWCNTs as seen in Fig. 5b1 are in the range of 13–15 nm, while in the case of NiO-MWCNTs the nickel oxide particles are in the range of 8–10 nm. The presence of the nanoparticles only on the surface of the nanotubes indicates that the nanoparticles are strongly anchored onto their surface. The compositional purity of the impregnated and the calcined composites were investigated by EDX (not shown) and found that only nickel is present apart from carbon and oxygen, which shows that there are no impurities in the product. In all the cases average nickel mass percentage was in

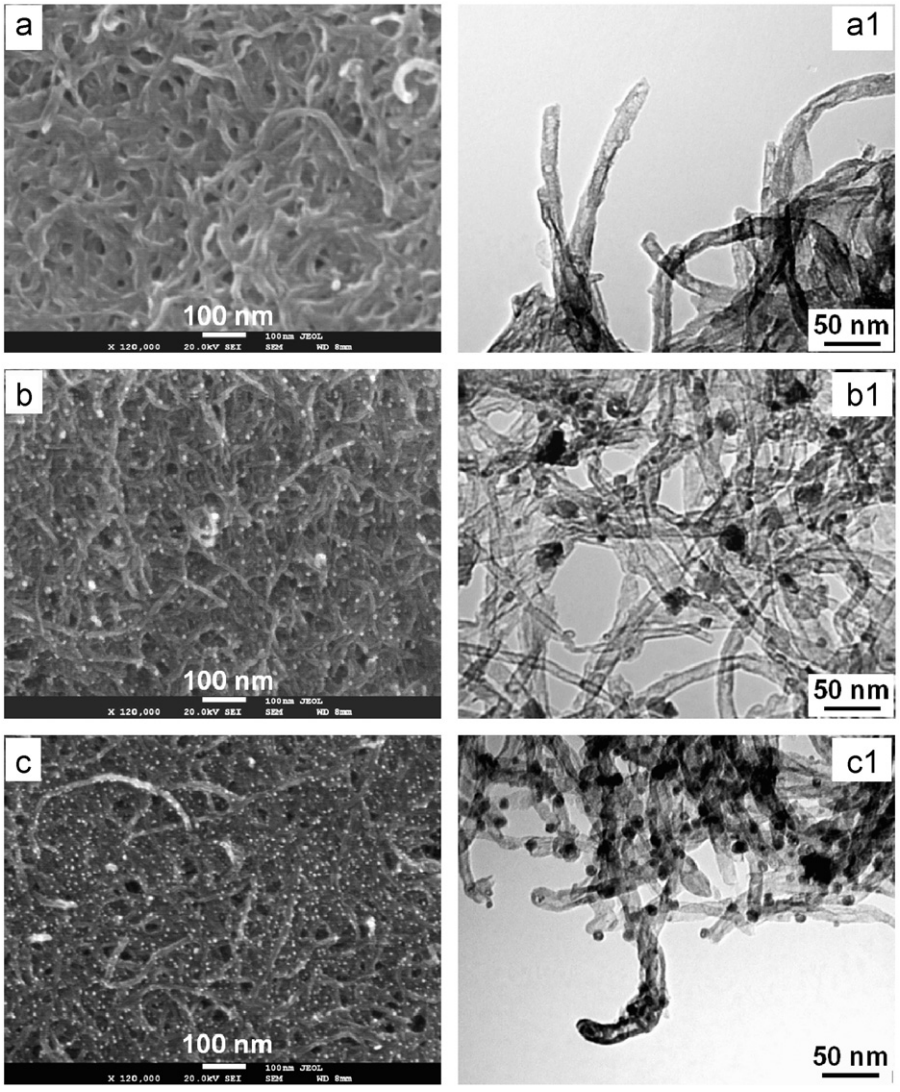

Fig. 5. FEG-SEM images of (a) NAA-MWCNTs, (b) Ni-MWCNTs and (c) NiO-MWCNTs. TEM images of (a1) NAA-MWCNTs, (b1) Ni-MWCNTs and (c1) NiO-MWCNTs.

the range of 10–12% indicating that most of the NAA utilized for the impregnation process is incorporated in the final products.

The thermal decomposition behaviors of all the samples were investigated by TGA in a flowing nitrogen atmosphere is shown in Fig. 6. Fig. 6a and b presents the TGA patterns of pristine and O-MWCNTs, respectively. In the case of pristine MWCNTs it is clearly seen that the CNTs slowly start degrading at a temperature around 650 °C; whereas in the case of O-MWCNTs, the weight loss was observed in several steps starting from 100 °C up to 750 °C and further. The total weight loss observed was about 30% for O-MWCNTs. First stage of weight loss was observed up to a temperature of 150 °C, corresponding to the evaporation of the adsorbed water. The second stage from 150 to 350 °C is ascribed to the decarboxylation due to the carboxylic groups present on the walls of CNT. The weight loss in the range between 350 °C and 500 °C can be explained by the elimination of hydroxyl functionalities present on the surface of MWCNTs. For the temperatures higher than 500 °C the thermal degradation correspond to the thermal oxidation of the remaining disordered carbon [17]. Fig. 6c represents the thermograms of pure NAA, which exhibits mainly two stages of degradation on weight loss at 289 °C having 40% weight loss and the other stage at 420 °C having 28% weight loss [36]. Small degradation on weight loss observed at 179 °C.

Since, major weight loss was observed around 420 °C, possibly the NAA is decomposed to form NiO at this stage. Hence NAA-MWCNTs were calcined around 400 °C in nitrogen atmosphere which gave rise to NiO-MWCNTs composites as evidenced by PXRD pattern shown earlier (Fig. 2c). However, as shown in Fig. 6d, a slight difference in weight loss pattern was observed for the TGA of NAA-MWCNTs compared to the O-MWCNTs. Here too we see that the decomposition pattern of NAA-MWCNTs is similar to that of NAA except that the weight loss percentage is different due to the presence of CNTs in the composites.

Possible formation mechanism of nickel and nickel oxide decorated CNTs can be explained as represented in Scheme 1. This work demonstrates the feasibility of decorating CNTs with nickel and nickel oxide nanocrystals via the calcination of impregnated NAA precursors in xylene solvent in hydrogen and nitrogen atmospheres, respectively. The CNT-coating mechanism, as schematically illustrated, may be closely associated with the wetting of oxygen-functionalized CNT surfaces with the precursor NAA. We believe that refluxing of NAA in xylene played a pivotal role in decorating CNTs with NAA as elevated temperature may have given impetus for the NAA to anchor on the defect sites created

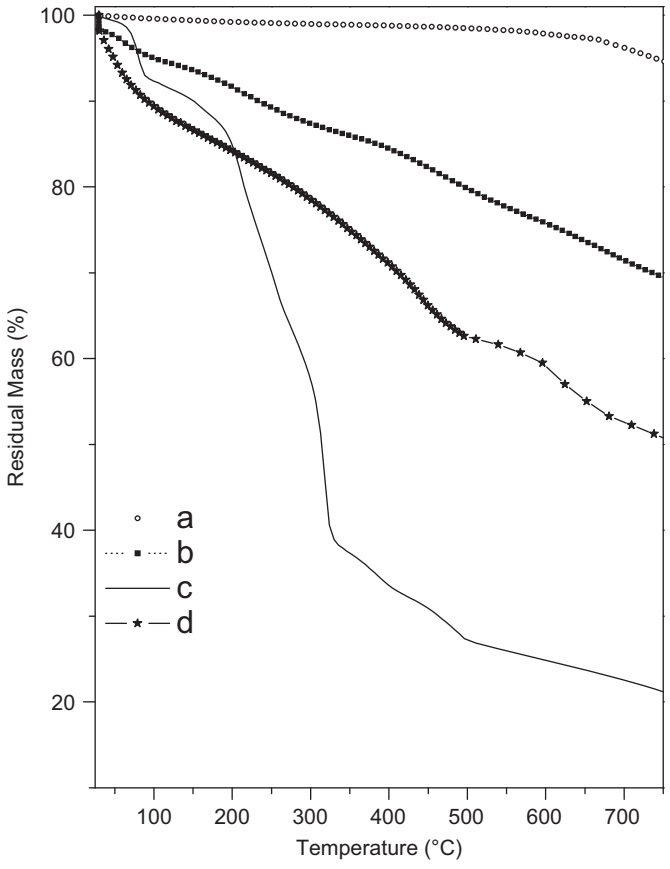

Fig. 6. TGA curves of (a) pristine MWCNTs, (b) O-MWCNTs and (c) NAA, (d) NAA-MWCNTs in nitrogen.

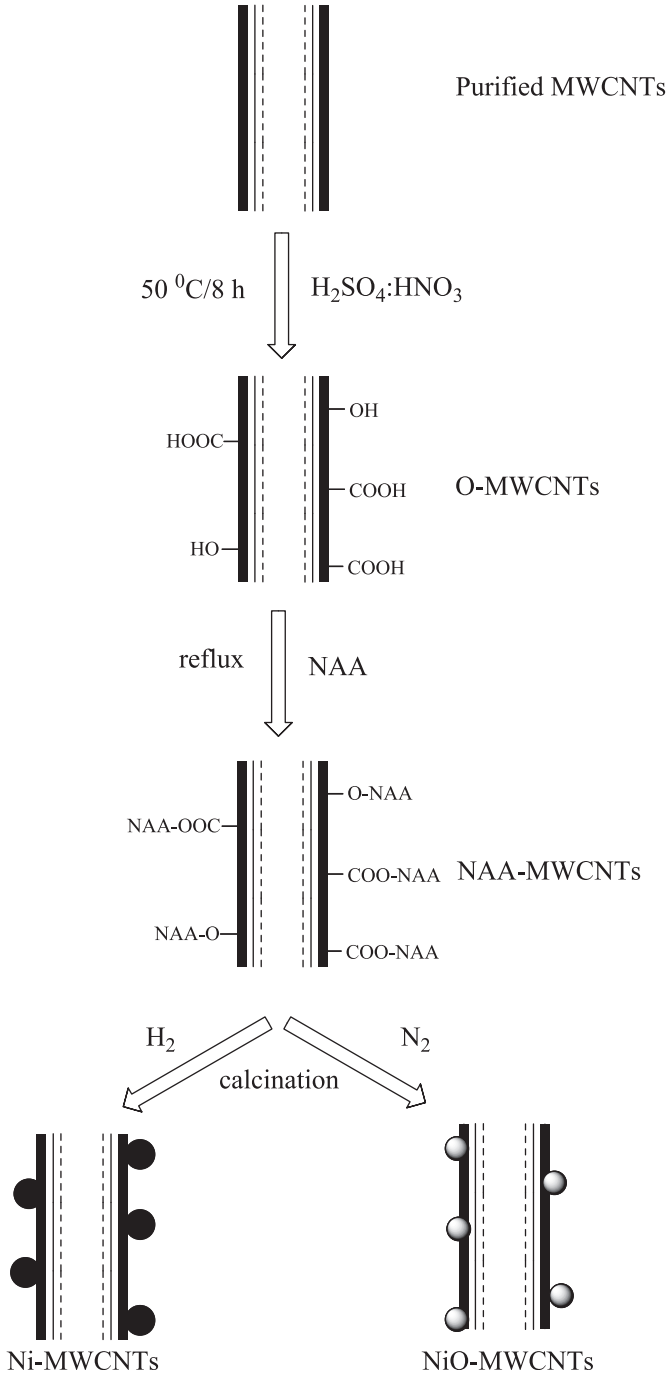

Scheme 1. Schematic illustration of the various steps involved to obtain the final products.

during the acid treatment of MWCNTs. It is well known that chemical oxidation using sulfuric and nitric acid mixture can create various functional groups, such as –COOH, –OH and –C=C at the defective sites on the nanotubes wall. They act as active sites for metal cations to attach during the impregnation process. When, the as obtained NAA-MWCNTs were calcined at certain temperatures in suitable atmospheres such as hydrogen and nitrogen led to the decomposition of the NAA trapped on the surfaces of CNTs and the formation of respective metal and metal oxide nanocrystals. As a consequence, CNTs were readily decorated with uniform nickel and nickel oxide nanocrystals. The final products were confirmed by different techniques used for the characterization.

4. Conclusions

A facile and alternative method for the synthesis of nickel and nickel oxide nanoparticles decorated on MWCNTs was described using NAA for the first time. The metal/metal oxide-carbon nanotube composites were synthesized by impregnation of carbon nanotubes with NAA metal precursor followed by calcination at suitable temperatures and atmospheres. The chemical impregnation process led to the homogeneously dispersed nickel and nickel oxide nanocrystals on the surface of MWCNTs, and the particles were found to possess an average size of 8–15 nm. This process implied a simple route to prepare Ni and NiO nanocrystals supported on CNTs through tuning the experimental conditions. Both the decorated nanocrystals on CNTs have potential applications in heterogeneous catalysis and semiconductor industries.

Acknowledgments

BRV thanks the Belgian National Fund for Scientific Research (FNRS) for the postdoctoral fellowship (Grant number 2.4550.09).

References

[1] V. Selvaraj, M. Vinoba, M. Alagar, J. Colloid Interface Sci. 322 (2008) 537.
[2] Y. Tang, D. Yang, F. Qin, J. Hu, C. Wang, H. Xu, J. Solid State Chem. 182 (2009) 2279.
[3] G.P. Jin, Y.F. Ding, P.P. Zheng, J. Power Sources 166 (2007) 80.
[4] V. Selvaraj, A.N. Grace, M. Alagar, J. Colloid Interface Sci. 333 (2009) 254.
[5] P.J.F. Harris, Carbon Nanotube Science, Cambridge University Press, Cambridge, 2009 (p. 146–199).
[6] S. Ijima, Physica B 323 (2002) 1.
[7] H.S. Park, T.J. Park, Y.S. Huh, B.G. Choi, S. Ko, S.Y. Lee, W.H. Hong, J. Colloid Interface Sci. 350 (2010) 453.
[8] P. Avouris, Chem. Phys. 281 (2002) 429.
[9] M. Endo, T. Hayashi, Y.A. Kim, M. Terrones, M.S. Dresselhaus, Phil. Trans. R. Soc. London A 362 (2004) 2223.
[10] R.H. Baughman, A.A. Zakhidov, W.A. de Heer, Science 297 (2002) 787.
[11] P. Ayala, F.L. Freire Jr, L. Gu, D.J. Smith, I.G. Solórzano, D.W. Macedo, J.B. Vander Sande, H. Terrones, J. Rodriguez-Manzo, M. Terrones, Chem. Phys. Lett. 431 (2006) 104.
[12] H.L. Zhuang, G.P. Zheng, A.K. Soh, Comp. Mater. Sci. 43 (2008) 823.
[13] M. Olek, M. Hilgendorff, M. Giersig, Colloids Surfaces A: Physicochem. Eng. Aspects 292 (2007) 83.
[14] S. Kundu, Y. Wang, W. Xia, M. Muhler, J. Phys. Chem. C 112 (2008) 16869.
[15] N.T. Hung, I.V. Anoshkin, A.P. Dementjev, D.V. Katorov, E.G. Rakov, Inorg. Mater 44 (2008) 219.
[16] C. Wang, G. Zhou, H. Liu, J. Wu, Y. Qiu, B.L. Gu, W. Duan, J. Phys. Chem. B 110 (2006) 10266.
[17] V. Datsyuk, M. Kalyva, K. Papagelis, J. Parthenios, D. Tasis, A. Siokou, I. Kallitsis, C. Galiotis, Carbon 46 (2008) 833.
[18] G. Zhang, S. Sun, D. Yang, J.P. Dodelet, E. Sacher, Carbon 46 (2008) 196.
[19] S.H. Su, W.T. Chiang, C.C. Lin, M. Yokoyama, Physica. E 40 (2008) 2322.
[20] E. Unger, G.S. Duesberg, M. Liebau, A.P. Graham, R. Seidel, F. Kreupl, W. Hoenlein, Appl. Phys. A 77 (2003) 735.
[21] X.H. Chen, C.S. Chen, H.N. Xiao, H.B. Liu, L.P. Zhou, S.L. Li, G. Zhang, Tribol. Int. 39 (2006) 22.
[22] J. Cheng, X. Zhang, Y. Ye, J. Solid State Chem. 179 (2006) 91.
[23] J.C. De Jesus, I. González, A. Quevedo, T. Puerta, J. Mol. Catal. A 228 (2005) 283.
[24] K.Y. Lin, W.T. Tsai, J.K. Chang, J. Int., Hydrogen Energy 35 (2010) 7555.
[25] C.T. Hsieh, Y.W. Chou, W.Y. Chen, J. Solid State Electrochem. 12 (2008) 663.
[26] J. Yan, Z. Fan, T. Wei, J. Cheng, B. Shao, K. Wang, L. Song, M. Zhang, J. Power Sources 194 (2009) 1202.
[27] M. Jayalakshmi, M.M. Rao, N. Venugopal, K.B. Kim, J. Power Sources 166 (2007) 578.
[28] A. Oki, L. Adams, Z. Luo, Inorg. Chem. Commun. 11 (2008) 275.
[29] M.K.S. Li, P. Gao, P-L. Yue, X. Hu, Sep. Purif. Technol. 67 (2009) 238.
[30] S.V. Mahajan, J. Cho, M.S.P. Shaffer, A.R. Boccaccini, J.H. Dickerson, J. Eur. Ceram. Soc. 30 (2010) 1145.
[31] E. Titus, N. Ali, G. Cabral, J. Gracio, P.R. Babu, M.J. Jackson, J. Mater. Eng. Perform. 15 (2006) 182.
[32] F. Liu, X.B. Zhang, D. Haussler, W. Jager, G.F. Yi, J.P. Cheng, X.Y. Tao, Z.Q. Luo, S.M. Zhou, J. Mater. Sci. 41 (2006) 4523.
[33] J.F. Moulder, W.F. Stickle, P.E. Sobol, K.D. Bomben, Handbook of X-Ray Photoelectron Spectroscopy, Perkin-Elmer, Eden, Paris, 1992.
[34] X. Tan, M. Fang, C. Chen, S. Yu, X. Wang, Carbon 46 (2008) 1741.
[35] G.G. Couto, J.J. Klein, W.H. Schreiner, D.H. Mosca, A.J.A. de Oliveira, A.J.G. Zarbin, J. Colloid Interface Sci. 311 (2007) 461.
[36] R. Molina, G. Poncelet, J. Phys. Chem. B 103 (1999) 11290.